Interplay of Orbital and Relativistic Effects in Bismuth Oxyhalides: BiOF, BiOCl, BiOBr, and BiOI

Alex M. Ganose,[†,‡] Madeleine Cuff,[†] Keith T. Butler,[∥] Aron Walsh,[∥,§] and David O. Scanlon[*,†,‡]

[†]Kathleen Lonsdale Materials Chemistry, Department of Chemistry, University College London, 20 Gordon Street, London WC1H 0AJ, United Kingdom

[‡]Diamond Light Source Ltd., Diamond House, Harwell Science and Innovation Campus, Didcot, Oxfordshire OX11 0DE, United Kingdom

[∥]Centre for Sustainable Chemical Technologies and Department of Chemistry, University of Bath, Claverton Down, Bath BA2 7AY, United Kingdom

[§]Global E³ Institute and Department of Materials Science and Engineering, Yonsei University, Seoul 120-749, Korea

S *Supporting Information*

The optoelectronic properties of bismuth oxyhalides have led to their utility in applications such as pigments in the cosmetics industry,[1,2] pharmaceuticals,[3,4] phosphors,[5] gas sensors,[6] and catalysis.[7,8] Over the past decade, interest in this family of materials has rapidly increased, fuelled by reports of their excellent photocatalytic activity.[9−16] They have been studied as stand-alone photocatalysts,[9,10,17] quaternary alloys,[18,19] and interfaced with other photocatalytically active materials.[20−22] To date, however, an understanding of the chemical trends underpinning these successes is lacking.

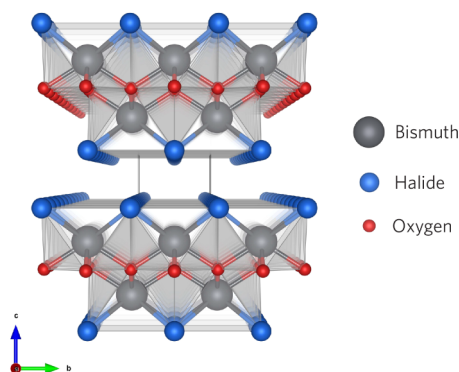The BiOX series, shown in Figure 1, crystallize in the tetragonal Matlockite structure,[23,24] which can be considered

Figure 1. Crystal structure of the BiOX systems (space group P4/nmm, D_{4h} symmetry) with stoichiometric X−Bi−O−Bi−X bilayers stacked along the c axis.

the simplest form of the Sillén-type structure and is commonly expressed as $[M_2O_2][X_m]$.[25] The crystal lattice consists of fluorite-like $[M_2O_2]$ layers sandwiched between double halide $[X_m]$ layers, to form [X−Bi−O−Bi−X] sheets, stacked in the [001] direction, with the structure held together by nonbonding van der Waals interactions along the [001] direction. It has been proposed that this structure type imparts an internal static electric field between the $[M_2O_2]^{2+}$ and double $[X]^-$ slab along the [001] direction, which aids efficient separation of the photogenerated electron−hole pairs.[9,10,26,27]

In this communication, we investigate the BiOX (X = F, Cl, Br, and I) series using hybrid density functional theory with explicit treatment of spin−orbit coupling effects and dispersion interactions. First, we resolve the band gap trends, where values between 3.5−3.6 eV, 2.9−3.4 eV, 2.3−2.9 eV, and 1.8−2.1 eV for BiOF, BiOCl, BiOBr, and BiOI, had been reported.[9,11,12,28−32] We separate the roles of relativistic and chemical effects in determining the magnitude of the gaps and also the absolute band energies, which provides guidance for designing tailored photocatalysts.

First-principles calculations were performed in the framework of density functional theory (DFT). Special attention was paid to electron−electron interactions (using the screened hybrid HSE06 functional),[33,34] relativistic effects (using scalar relativistic PAW pseudopotentials[35,36] and spin−orbit coupling, SOC), and dispersion interactions (the DFT-D3 correction[37,38]). All solid-state calculations were performed in a plane-wave basis set using the code VASP.[39,40]

Complete structural optimizations (forces < 0.01 eV Å⁻¹) were performed at a series of volumes in order to calculate the equilibrium lattice parameters. Convergence with respect to k-point sampling and plane wave energy was checked, with a cutoff of 520 eV and a k-point density of 0.04 k Å found to be sufficient. To align the electronic band energies to the vacuum level, a surface−slab model (15 Å vacuum spacing) was constructed and the corresponding electrostatic potential averaged along the c-direction, using the MacroDensity package.[41−43] The (100) surface was chosen as it is a nonpolar termination that results in minimal bond cleavage and does not produce undesirable surface states.

The predicted lattice parameters for the BiOX series are shown in Table 1. The results are in good agreement with previous experimental measurements (within 1%),[11,23,24] taking into account that the experimental data is mostly for room temperature. The inclusion of the nonlocal dispersion correction was vital for achieving an accurate equilibrium geometry, especially as we descend down the halide group, as

Table 1. Calculated Structural and Electronic Properties of the BiOX Series[a]

material	a	c	E_g	IP	EA
BiOF	3.72 (−1.0%)	6.20 (−0.5%)	4.18	8.23	3.87
BiOCl	3.87 (−0.5%)	7.42 (+0.9%)	3.37	7.94	4.35
BiOBr	3.90 (−0.5%)	8.14 (−0.5%)	2.82	7.55	4.65
BiOI	3.98 (−0.3%)	9.15 (0.0%)	2.00	7.03	5.03

[a]All lattice vectors are given in Å (% error with respect to room temperature diffraction measurements in parentheses), with the band gap, ionisation potential (IP), and electron affinity (EA) in eV.

shown in Table S1 of the Supporting Information. Without this interaction, the error in the c parameter can grow to as much as 1 Å.

Similar to the hybrid halide perovskites[44−46] and topological insulators[47,48] which are also composed of atoms with high atomic number, it is expected that relativistic effects should play a large role in determining the electronic structure of these materials. The band structures of the BiOX series with and without the explicit treatment of SOC are plotted in Figure 2a−d. The inclusion of SOC was found to result in a net band gap reduction independent of chemical composition, with the conduction band minimum (CBM) of BiOF, BiOCl, BiOBr, and BiOI lowered by 0.39, 0.24, 0.24, and 0.22 eV, respectively. The valence band maximum (VBM) is less affected by SOC effects, with only BiOI experiencing a significant upward shift of 0.11 eV, due to larger relativistic effect on I states as group 17 is descended. As such, the effect of SOC is insufficient in explaining the trend in band gap across the series.

Instead, analysis of the total and partial (ion decomposed) density of states for the BiOX series, shown in Figure 3, is instructive in explaining the trend in optical response seen in experiment. For BiOF, the top of the valence band is dominated by O 2p states, with the F 2p states found at higher binding energies. As the halide anion changes upon moving down group 17, the contribution of the halide p states to the VBM increases, ultimately dominating the VBM in BiOI. In all cases, the conduction band is dominated by Bi p states. It is therefore clear that the valence band composition dictates the band gap reduction down the series, in line with the binding energy of the halide p orbitals. The Bi 6s states are mainly found at the *bottom* of the valence band but additionally provide a small contribution toward the *top* of the valence band. Consistent with the revised lone pair theory,[49−51] the orbital overlap * of Bi 6s* with the O 2p and halide p states is not sufficient to warrant a structural distortion, meaning the Bi is perfectly octahedral in the Matlockite structure.

From the band structures shown in Figure 2 it can be seen that the fundamental band gaps across the BiOX series are indirect. The CBM of BiOF, BiOCl, and BiOBr appears at the Z point, with the VBM positioned between Z → R. For BiOI, the CBM is situated between Γ → R, and the VBM is again situated between Z → R. The fundamental indirect band gaps are 4.18, 3.37, 2.82, and 2.00 eV for BiOF, BiOCl, BiOBr, and BiOI, respectively, which, in all cases except BiOF, are in excellent agreement with experimental measurements.[12] The calculated hole effective masses are relatively large; however, they are considerably smaller in BiOCl and BiOBr (0.8 m_e and 0.7 m_e) than in BiOF and BiOI (12.5 m_e and 1.9 m_e). The dispersion of the conduction band is noticeably less along Z → Γ (in the [001] direction) compared to Z → R ([010]), which is to be expected as Z → Γ spans across the [X−Bi−O−Bi−X] sheets, whereas Z → R is in the plane of the layers. This is reflected in the electron effective masses of BiOF, BiOCl, and BiOBr, which are significantly lower in the Z → Γ direction (0.5 m_e, 0.3 m_e, and 0.3 m_e, respectively) than along Z → R (1.0 m_e, 2.4 m_e, and 0.6 m_e, respectively).

To understand the effect of varying the halide ion on the fundamental band alignments of the BiOX series, we have plotted the valence band alignment of these materials using the slab model,[52] with the results shown in Figure 4. As expected based on the relative energy levels of the halide p-orbitals, the ionization potential (IP) of the BiOX series gets smaller as we descend down group 17. The Bi-based conduction band is also lowered on descending group 17, which can be rationalized due to the Bi p states experiencing a different Madelung potential as the ionic radius of the halide increases on moving down the group.

The alignment helps to explain some of the puzzling experimental observations in the literature. The BiOX series have been reported to display p-type conductivity[15] but unusually to also exhibit n-type behavior.[54] Our calculated electron affinity (EA) for BiOI of 5.2 eV is consistent with the EAs exhibited by many excellent n-type materials.[55−57] The larger EA of BiOI also results in a reduced overpotential for O_2/oxygen anion splitting and can explain why BiOI is not as active for the degradation of rhodamine B than BiOBr and BiOCl.[12,58] In addition alloys between BiOCl/BiOBr[59] and BiOBr/BiOI[60] have been demonstrated to outperform the individual materials, and this can be rationalized by the ability to tailor the band edges in order to obtain an enhanced electronic alignment in the alloys.

We have demonstrated the key role of the halide anion in determining the electronic structure and properties of the
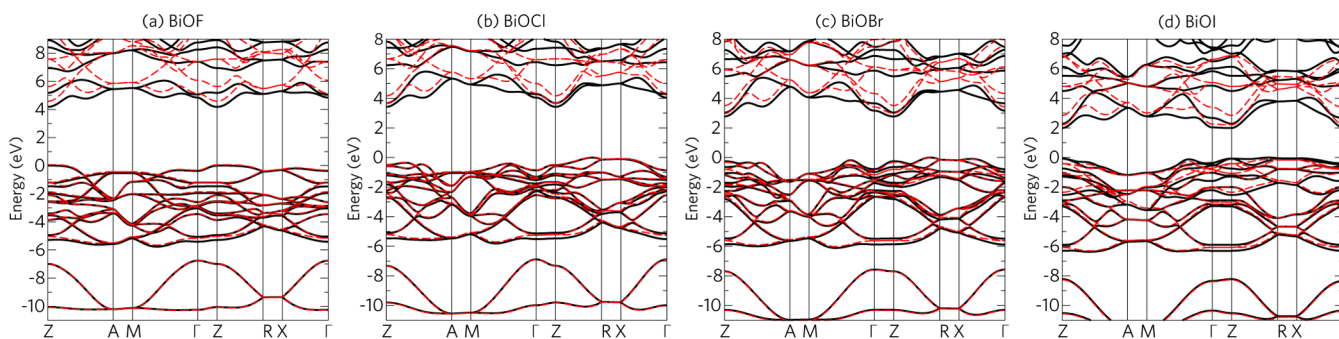

Figure 2. Scalar relativistic (dashed lines) and fully relativistic (black lines) electronic band structures of the BiOX series with the hybrid HSE06 functional. The highest occupied state (including spin−orbit coupling) is set to 0 eV.
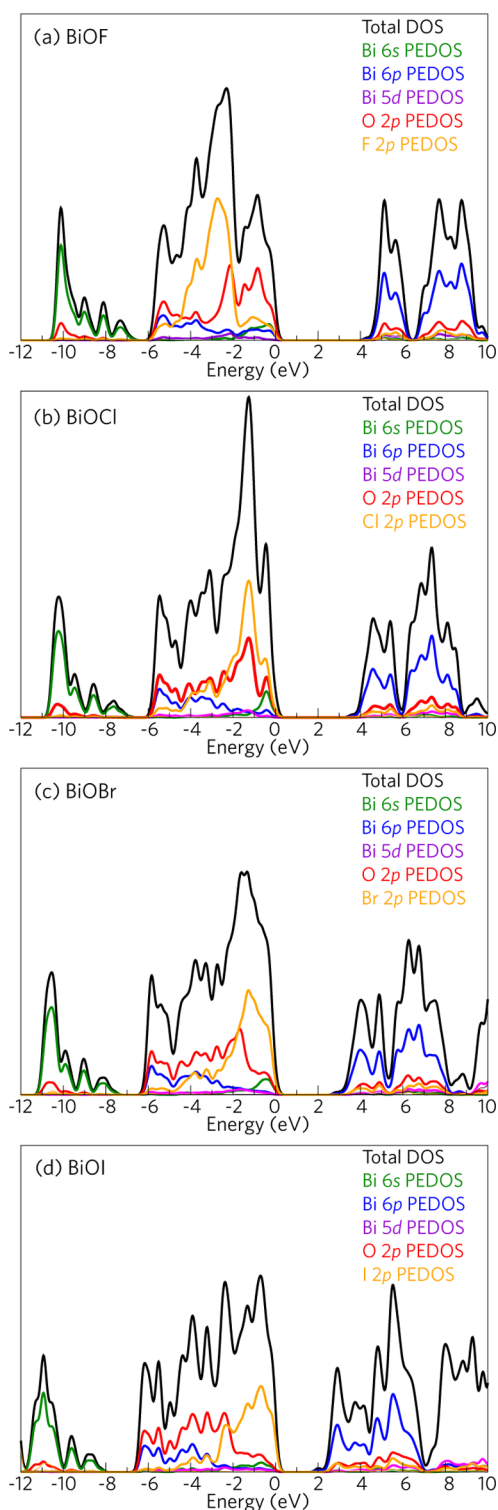
Figure 3. Fully relativistic (HSE06+SOC) electronic density of states (DOS), including projections onto ion-centered atomic orbitals (PEDOS). The highest occupied state is set to 0 eV.

Figure 4. Calculated valence band alignment of the BiOX series (HSE including spin−orbit coupling). The vacuum level was aligned to the (001) surface in a slab calculation with a vacuum thickness of 15 Å. The electrostatic potentials were aligned and checked using the package MacroDensity.[53]

■ ASSOCIATED CONTENT

ⓈSupporting Information

The Supporting Information is available free of charge on the ACS Publications website at DOI: 10.1021/acs.chemmater.6b00349.

Comparison of lattice parameters and bond lengths calculated with and without Grimme's D3 dispersion correction (PDF)

■ AUTHOR INFORMATION

Corresponding Author

*(D.O.S.) E-mail: d.scanlon@ucl.ac.uk.

Notes

The authors declare no competing financial interest.

■ ACKNOWLEDGMENTS

■ REFERENCES

(1) Auer, G.; Griebler, W.; Jahn, B. In *Industrial Inorganic Pigments*; Buxbaum, G., Pfaff, G., Eds.; Wiley-VCH Verlag GmbH & Co. KGaA: Weinheim, 2005; pp 129−130.

(2) Pfaff, G.; Reynders, P. Angle-Dependent Optical Effects Deriving from Submicron Structures of Films and Pigments. *Chem. Rev.* **1999**, *99*, 1963−1982.

bismuth oxyhalide series. The range of functionality will be further extended by also changing the chalcogenide anion, as suggested by recent reports of topological electronic states and relativistic band splitting in the bismuth tellurihalides. As such, this extended family of compounds merits further investigation.
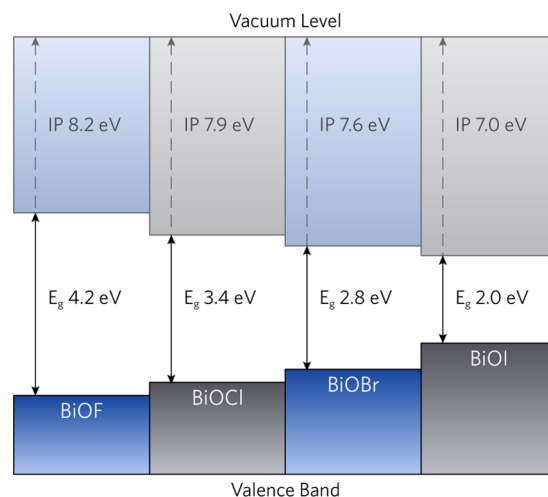
(3) Rotmensch, J.; Whitlock, J.; Dietz, M.; Hines, J.; Reba, R.; Horwitz, E.; Harper, P. Development of 212-BiOCl as a new therapeutic modality against microscopic carcinoma. *Abstr. Pap. Am. Chem. Soc.* **1998**, U926–U926.

(4) Briand, G. G.; Burford, N. Bismuth Compounds and Preparations with Biological or Medicinal Relevance. *Chem. Rev.* **1999**, *99*, 2601–2658.

(5) Rabatin, J. G. Bismuth Activated Rare Earth Oxybromide Phosphors and X-Ray Image Converters Utilizing Said Phosphors. U.S. Patent 4,068,129, 1978.

(6) Michel, C. R.; Contreras, N. L. L.; Martínez-Preciado, A. H. Gas Sensing Properties of Nanostructured Bismuth Oxychloride. *Sens. Actuators, B* **2011**, *160*, 271–277.

(7) Kijima, N.; Matano, K.; Saito, M.; Oikawa, T.; Konishi, T.; Yasuda, H.; Sato, T.; Yoshimura, Y. Oxidative Catalytic Cracking of N-Butane to Lower Alkenes over Layered BiOCl Catalyst. *Appl. Catal., A* **2001**, *206*, 237–244.

(8) Ghosh, R.; Maiti, S.; Chakraborty, A. Facile Catalyzed Acylation of Heteroatoms Using $BiCl_3$ Generated in situ From the Procatalyst BiOCl and Acetyl Chloride. *Tetrahedron Lett.* **2004**, *45*, 6775–6778.

(9) Zhang, K.-L.; Liu, C.-M.; Huang, F.-Q.; Zheng, C.; Wang, W.-D. Study of the Electronic Structure and Photocatalytic Activity of the BiOCl Photocatalyst. *Appl. Catal., B* **2006**, *68*, 125–129.

(10) Zhang, J.; Shi, F.; Lin, J.; Chen, D.; Gao, J.; Huang, Z.; Ding, X.; Tang, C. Self-Assembled 3-D Architectures of BiOBr as a Visible Light-Driven Photocatalyst. *Chem. Mater.* **2008**, *20*, 2937–2941.

(11) Zhang, X.; Ai, Z.; Jia, F.; Zhang, L. Generalized One-Pot Synthesis, Characterization,and Photocatalytic Activity of Hierarchical BiOX (x= Cl, Br, I) Nanoplate Microspheres. *J. Phys. Chem. C* **2008**, *112*, 747–753.

(12) An, H.; Du, Y.; Wang, T.; Wang, C.; Hao, W.; Zhang, J. Photocatalytic Properties of BiOX (X= Cl, Br, and I). *Rare Met.* **2008**, *27*, 243–250.

(13) Chai, S. Y.; Kim, Y. J.; Jung, M. H.; Chakraborty, A. K.; Jung, D.; Lee, W. I. Het-erojunctioned $BiOCl/Bi_2O_3$, a New Visible Light Photocatalyst. *J. Catal.* **2009**, *262*, 144–149.

(14) Chang, X.; Huang, J.; Cheng, C.; Sui, Q.; Sha, W.; Ji, G.; Deng, S.; Yu, G. BiOX (X = Cl, Br, I) Photocatalysts Prepared Using $NaBiO_3$ as the Bi Source: Characterization and Catalytic Performance. *Catal. Commun.* **2010**, *11*, 460–464.

(15) Cheng, H.; Huang, B.; Dai, Y. Engineering BiOX (X= Cl, Br, I) Nanostructures for Highly Efficient Photocatalytic Applications. *Nanoscale* **2014**, *6*, 2009–2026.

(16) Bhachu, D. S.; Moniz, S. J. A.; Sathasivam, S.; Scanlon, D. O.; Walsh, A.; Bawaked, S. M.; Mokhtar, M.; Obaid, A. Y.; Parkin, I. P.; Tang, J.; Carmalt, C. J. Bismuth Oxyhalides: Synthesis, Structure and Photoelectrochemical Activity. *Chem. Sci.* **2016**, DOI: 10.1039/C6SC00389C.

(17) Zhang, H.; Liu, L.; Zhou, Z. First-Principles Studies on Facet-Dependent Photocatalytic Properties of Bismuth Oxyhalides (BiOXs). *RSC Adv.* **2012**, *2*, 9224–9229.

(18) Gnayem, H.; Sasson, Y. Hierarchical Nanostructured 3D Flowerlike $BiOCl_xBr_{1-x}$ Semi- conductors with Exceptional Visible Light Photocatalytic Activity. *ACS Catal.* **2013**, *3*, 186–191.

(19) Zhang, H.; Liu, L.; Zhou, Z. Towards Better Photocatalysts: First-Principles Studies of the Alloying Effects on the Photocatalytic Activities of Bismuth Oxyhalides Under Visible Light. *Phys. Chem. Chem. Phys.* **2012**, *14*, 1286–1292.

(20) Li, J.; Yu, Y.; Zhang, L. Bismuth Oxyhalide Nanomaterials: Layered Structures Meet Photocatalysis. *Nanoscale* **2014**, *6*, 8473–8488.

(21) Shamaila, S.; Sajjad, A. K. L.; Chen, F.; Zhang, J. WO₃/BiOCl, a novel heterojunction as visible light photocatalyst. *J. Colloid Interface Sci.* **2011**, *356*, 465–472.

(22) Shenawi-Khalil, S.; Uvarov, V.; Fronton, S.; Popov, I.; Sasson, Y. A Novel Heterojunc-tion BiOBr/Bismuth Oxyhydrate Photocatalyst with Highly Enhanced Visible Light Photocatalytic Properties. *J. Phys. Chem. C* **2012**, *116*, 11004–11012.

(23) Keramidas, K.; Voutsas, G.; Rentzeperis, P. The Crystal Structure of BiOCl. *Z. Kristallogr. - Cryst. Mater.* **1993**, *205*, 35–40.

(24) Bannister, F.; Hey, M. The Crystal Structure Of The Bismuth Oxyhalides. *Mineral. Mag.* **1935**, *24*, 49–58.

(25) Kusainova, A. M.; Zhou, W.; Irvine, J. T.; Lightfoot, P. Layered Intergrowth Phases Bi_4MO_8X (X= Cl, M= Ta and X= Br, M= Ta or Nb): Structural and Electrophysical Characterization. *J. Solid State Chem.* **2002**, *166*, 148–157.

(26) Ai, Z.; Ho, W.; Lee, S.; Zhang, L. Efficient Photocatalytic Removal of NO in Indoor Air with Hierarchical Bismuth Oxybromide Nanoplate Microspheres Under Visible Light. *Environ. Sci. Technol.* **2009**, *43*, 4143–4150.

(27) Henle, J.; Simon, P.; Frenzel, A.; Scholz, S.; Kaskel, S. Nanosized BiOX (X= Cl, Br, I) Particles Synthesized in Reverse Microemulsions. *Chem. Mater.* **2007**, *19*, 366–373.

(28) Wang, W.; Huang, F.; Lin, X. xBiOI—(1−x)BiOCl as efficient visible-light-driven photocatalysts. *Scr. Mater.* **2007**, *56*, 669–672.

(29) Wang, W.; Huang, F.; Lin, X.; Yang, J. Visible-Light-Responsive Photocatalysts xBiOBr—(1−x)BiOI. *Catal. Commun.* **2008**, *9*, 8–12.

(30) Chen, L.; Yin, S.-F.; Huang, R.; Zhou, Y.; Luo, S.-L.; Au, C.-T. Facile Synthesis of BiOCl Nano-Flowers of Narrow Band Gap and their Visible-Light-Induced Photocatalytic Property. *Catal. Commun.* **2012**, *23*, 54–57.

(31) Su, W.; Wang, J.; Huang, Y.; Wang, W.; Wu, L.; Wang, X.; Liu, P. Synthesis and Catalytic Performances of a Novel Photocatalyst BiOF. *Scr. Mater.* **2010**, *62*, 345–348.

(32) Deng, H.; Wang, J.; Peng, Q.; Wang, X.; Li, Y. Controlled Hydrothermal Synthesis of Bismuth Oxyhalide Nanobelts and Nanotubes. *Chem. - Eur. J.* **2005**, *11*, 6519–6524.

(33) Heyd, S.; Scuseria, G. E.; Ernzerhof, M. Hybrid Functionals Based on a Screened Coulomb Potential. *J. Chem. Phys.* **2003**, *118*, 8207–8215.

(34) Krukau, A. V.; Vydrov, O. A.; Izmaylov, A. F.; Scuseria, G. E. Influence of the Exchange Screening Parameter on the Performance Of Screened Hybrid Functionals. *J. Chem. Phys.* **2006**, *125*, 224106.

(35) Blöchl, P. E. Projector Augmented-Wave Method. *Phys. Rev. B: Condens. Matter Mater. Phys.* **1994**, *50*, 17953.

(36) Kresse, G.; Joubert, D. From Ultrasoft Pseudopotentials to the Projector Augmented Wave Method. *Phys. Rev. B: Condens. Matter Mater. Phys.* **1999**, *59*, 1758–1775.

(37) Grimme, S. Accurate Description of van der Waals Complexes by Density Funcitonal Theory Including Empirical Corrections. *J. Comput. Chem.* **2004**, *25*, 1463–1473.

(38) Savory, C. N.; Palgrave, R. G.; Bronstein, H.; Scanlon, D. O. Spatial Electron-hole Separation in a One Dimensional Hybrid Organic−Inorganic Lead Iodide. *Sci. Rep.* **2016**, *6*, 20626.

(39) Kresse, G.; Furthmüller, J. Efficient Iterative Schemes for ab initio Total-Energy Calculations Using a Plane-wave Basis Set. *Phys. Rev. B: Condens. Matter Mater. Phys.* **1996**, *54*, 11169–11186.

(40) Kresse, G.; Hafner, J. *Ab Initio* Molecular-Dynamics Simulation of the Liquid-Metal−Amorphous-Semiconductor Transition in Germanium. *Phys. Rev. B: Condens. Matter Mater. Phys.* **1994**, *49*, 14251–14271.

(41) Walsh, A.; Butler, K. T. Prediction of Electron Energies in Metal Oxides. *Acc. Chem. Res.* **2014**, *47*, 364–372.

(42) Ganose, A. M.; Butler, K. T.; Walsh, A.; Scanlon, D. O. Relativistic Electronic Struc-ture and Band Alignment of BiSI and BiSeI: Candidate Photovoltaic Materials. *J. Mater. Chem. A* **2016**, *4*, 2060–2068.

(43) Brgoch, J.; Lehner, A. J.; Chabinyc, M.; Seshadri, R. Ab Initio Calculations of Band Gaps and Absolute Band Positions of Polymorphs of $RbPbI_3$ and $CsPbI_3$: Implications for Main-Group Halide Perovskite Photovoltaics. *J. Phys. Chem. C* **2014**, *118*, 27721–27727.

(44) Brivio, F.; Butler, K. T.; Walsh, A.; Van Schilfgaarde, M. Relativistic Quasiparticle Self-Consistent Electronic Structure of Hybrid Halide Perovskite Photovoltaic Absorbers. *Phys. Rev. B: Condens. Matter Mater. Phys.* **2014**, *89*, 155204.

(45) Even, J.; Pedesseau, L.; Jancu, J.-M.; Katan, C. Importance of Spin−Orbit Coupling in Hybrid Organic/Inorganic Perovskites for Photovoltaic Applications. *J. Phys. Chem. Lett.* **2013**, *4*, 2999−3005.

(46) Ganose, A. M.; Savory, C. N.; Scanlon, D. O. $(CH_3NH_3)_2Pb(SCN)_2I_2$: A More Stable Structural Motif for Hybrid Halide Photovoltaics? *J. Phys. Chem. Lett.* **2015**, *6*, 4594−4598.

(47) Zhang, H.; Liu, C.-X.; Qi, X.-L.; Dai, X.; Fang, Z.; Zhang, S.-C. Topological Insulators in Bi_2Se_3, Bi_2Te_3 and Sb_2Te_3 with a Single Dirac Cone on the Surface. *Nat. Phys.* **2009**, *5*, 438−442.

(48) Scanlon, D.; King, P.; Singh, R.; De La Torre, A.; Walker, S. M.; Balakrishnan, G.; Baumberger, F.; Catlow, C. Controlling Bulk Conductivity in Topological Insulators:Key Role of Anti-Site Defects. *Adv. Mater.* **2012**, *24*, 2154−2158.

(49) Waghmare, U.; Spaldin, N.; Kandpal, H.; Seshadri, R. First-Principles Indicators of Metallicity and Cation Off-Centricity in rhe IV-VI Rocksalt Chalcogenides of Divalent Ge, Sn, and Pb. *Phys. Rev. B: Condens. Matter Mater. Phys.* **2003**, *67*, 125111.

(50) Raulot, J.-M.; Baldinozzi, G.; Seshadri, R.; Cortona, P. An Ab-Initio Study of the rôle of Lone Pairs in the Structure and Insulator−Metal Transition in SnO and PbO. *Solid State Sci.* **2002**, *4*, 467−474.

(51) Walsh, A.; Watson, G. W. The Origin of the Stereochemically Active Pb(II) Lone Pair: DFT Calculations on PbO And PbS. *J. Solid State Chem.* **2005**, *178*, 1422−1428.

(52) Burton, L. A.; Walsh, A. Band Alignment in SnS Thin-Film Solar Cells: Possible Origin of the Low Conversion Efficiency. *Appl. Phys. Lett.* **2013**, *102*, 132111.

(53) Butler, K. T.; Hendon, C. H.; Walsh, A. Electronic Chemical Potentials of Porous Metal−Organic Frameworks. *J. Am. Chem. Soc.* **2014**, *136*, 2703−2706.

(54) Hahn, N. T.; Hoang, S.; Self, J. L.; Mullins, C. B. Spray Pyrolysis Deposition and Photoelectrochemical Properties of n-Type BiOI Nanoplatelet Thin Films. *ACS Nano* **2012**, *6*, 7712−7722.

(55) Scanlon, D. O.; Watson, G. W. On the Possibility of p-Type SnO_2. *J. Mater. Chem.* **2012**, *22*, 25236−25245.

(56) Frost, J. M.; Butler, K. T.; Brivio, F.; Hendon, C. H.; Van Schilfgaarde, M.; Walsh, A. Atomistic Origins of High-Performance in Hybrid Halide Perovskite Solar Cells. *Nano Lett.* **2014**, *14*, 2584−2590.

(57) Ganose, A. M.; Scanlon, D. O. Band Gap and Work Function Tailoring of SnO_2 for Improved Transparent Conducting Ability in Photovoltaics. *J. Mater. Chem. C* **2016**, *4*, 1467−1475.

(58) Chang, X.; Gondal, M.; Al-Saadi, A.; Ali, M.; Shen, H.; Zhou, Q.; Zhang, J.; Du, M.; Liu, Y.; Ji, G. Photodegradation of Rhodamine B Over Unexcited Semiconductor Compounds of BiOCl and BiOBr. *J. Colloid Interface Sci.* **2012**, *377*, 291−298.

(59) Zhang, J.; Xia, J.; Yin, S.; Li, H.; Xu, H.; He, M.; Huang, L.; Zhang, Q. Improvement of Visible Light Photocatalytic Activity Over Flower-Like BiOCl/BiOBr Microspheres Synthesized by Reactable Ionic Liquids. *Colloids Surf., A* **2013**, *420*, 89−95.

(60) Cao, J.; Xu, B.; Luo, B.; Lin, H.; Chen, S. Novel BiOI/BiOBr Heterojunction Photocatalysts with Enhanced Visible Light Photocatalytic Properties. *Catal. Commun.* **2011**, *13*, 63−68.